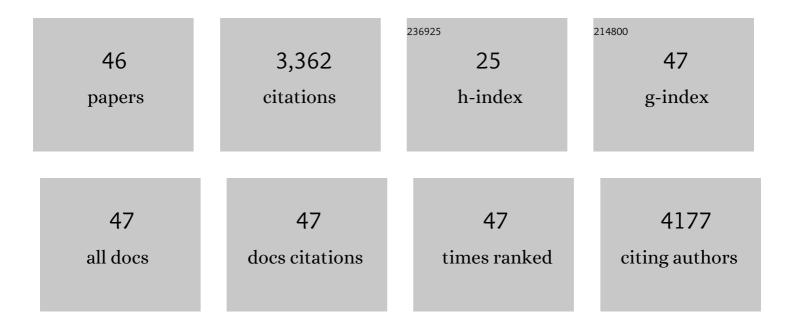
Eric P Visser

List of Publications by Year in descending order

Source: https://exaly.com/author-pdf/11248061/publications.pdf Version: 2024-02-01



#	Article	IF	CITATIONS
1	FDG PET and PET/CT: EANM procedure guidelines for tumour PET imaging: version 1.0. European Journal of Nuclear Medicine and Molecular Imaging, 2010, 37, 181-200.	6.4	1,147
2	The Netherlands protocol for standardisation and quantification of FDG whole body PET studies in multi-centre trials. European Journal of Nuclear Medicine and Molecular Imaging, 2008, 35, 2320-2333.	6.4	343
3	Spatial Resolution and Sensitivity of the Inveon Small-Animal PET Scanner. Journal of Nuclear Medicine, 2009, 50, 139-147.	5.0	175
4	Quantification, improvement, and harmonization of small lesion detection with state-of-the-art PET. European Journal of Nuclear Medicine and Molecular Imaging, 2017, 44, 4-16.	6.4	156
5	Image-Quality Assessment for Several Positron Emitters Using the NEMA NU 4-2008 Standards in the Siemens Inveon Small-Animal PET Scanner. Journal of Nuclear Medicine, 2010, 51, 610-617.	5.0	138
6	Chemotherapy Response Evaluation with 18F-FDG PET in Patients with Non-Small Cell Lung Cancer. Journal of Nuclear Medicine, 2007, 48, 1592-1598.	5.0	109
7	Methodological considerations in quantification of oncological FDG PET studies. European Journal of Nuclear Medicine and Molecular Imaging, 2010, 37, 1408-1425.	6.4	108
8	Glucose Metabolism in NSCLC Is Histology-Specific and Diverges the Prognostic Potential of 18FDG-PET for Adenocarcinoma and Squamous Cell Carcinoma. Journal of Thoracic Oncology, 2014, 9, 1485-1493.	1.1	107
9	PET in the management of locally advanced and metastatic NSCLC. Nature Reviews Clinical Oncology, 2015, 12, 395-407.	27.6	75
10	Comparison of image-derived and arterial input functions for estimating the rate of glucose metabolism in therapy-monitoring 18F-FDG PET studies. Journal of Nuclear Medicine, 2006, 47, 945-9.	5.0	70
11	A Curve-Fitting Approach to Estimate the Arterial Plasma Input Function for the Assessment of Glucose Metabolic Rate and Response to Treatment. Journal of Nuclear Medicine, 2009, 50, 1933-1939.	5.0	68
12	The Impact of Optimal Respiratory Gating and Image Noise on Evaluation of Intratumor Heterogeneity on ¹⁸ F-FDG PET Imaging of Lung Cancer. Journal of Nuclear Medicine, 2016, 57, 1692-1698.	5.0	67
13	Multicenter Harmonization of ⁸⁹ Zr PET/CT Performance. Journal of Nuclear Medicine, 2014, 55, 264-267.	5.0	63
14	Comparison of Tumor Volumes Derived from Glucose Metabolic Rate Maps and SUV Maps in Dynamic ¹⁸ F-FDG PET. Journal of Nuclear Medicine, 2008, 49, 892-898.	5.0	51
15	Amplitude-based optimal respiratory gating in positron emission tomography in patients with primary lung cancer. European Radiology, 2014, 24, 3242-3250.	4.5	51
16	Towards standardization of absolute SPECT/CT quantification: a multi-center and multi-vendor phantom study. EJNMMI Physics, 2019, 6, 29.	2.7	47
17	Dosimetric Analysis of ¹⁷⁷ Lu-cG250 Radioimmunotherapy in Renal Cell Carcinoma Patients: Correlation with Myelotoxicity and Pretherapeutic Absorbed Dose Predictions Based on ¹¹¹ In-cG250 Imaging. Journal of Nuclear Medicine, 2012, 53, 82-89.	5.0	45
18	SUV: From Silly Useless Value to Smart Uptake Value. Journal of Nuclear Medicine, 2010, 51, 173-175.	5.0	44

ERIC P VISSER

#	Article	IF	CITATIONS
19	Quantitative Assessment of Heterogeneity in Tumor Metabolism Using FDG-PET. International Journal of Radiation Oncology Biology Physics, 2012, 82, e725-e731.	0.8	35
20	Predictive patient-specific dosimetry and individualized dosing of pretargeted radioimmunotherapy in patients with advanced colorectal cancer. European Journal of Nuclear Medicine and Molecular Imaging, 2014, 41, 1593-602.	6.4	33
21	Semiautomatic methods for segmentation of the proliferative tumour volume on sequential FLT PET/CT images in head and neck carcinomas and their relation to clinical outcome. European Journal of Nuclear Medicine and Molecular Imaging, 2014, 41, 915-924.	6.4	31
22	Comparison of Tumor Uptake Heterogeneity Characterization Between Static and Parametric ¹⁸ F-FDG PET Images in Non–Small Cell Lung Cancer. Journal of Nuclear Medicine, 2016, 57, 1033-1039.	5.0	31
23	Using the NEMA NU 4 PET Image Quality Phantom in Multipinhole Small-Animal SPECT. Journal of Nuclear Medicine, 2011, 52, 1646-1653.	5.0	30
24	Chemotherapy Response Monitoring of Colorectal Liver Metastases by Dynamic Gd-DTPA–Enhanced MRI Perfusion Parameters and 18F-FDG PET Metabolic Rate. Journal of Nuclear Medicine, 2009, 50, 1777-1784.	5.0	29
25	Metal Artifact Reduction of CT Scans to Improve PET/CT. Journal of Nuclear Medicine, 2017, 58, 1867-1872.	5.0	29
26	PET-Based Human Dosimetry of ⁶⁸ Ga-NODAGA-Exendin-4, a Tracer for β-Cell Imaging. Journal of Nuclear Medicine, 2020, 61, 112-116.	5.0	26
27	Metabolic Subtyping of Pheochromocytoma and Paraganglioma by ¹⁸ F-FDG Pharmacokinetics Using Dynamic PET/CT Scanning. Journal of Nuclear Medicine, 2019, 60, 745-751.	5.0	21
28	Improving the Spatial Alignment in PET/CT Using Amplitude-Based Respiration-Gated PET and Respiration-Triggered CT. Journal of Nuclear Medicine, 2015, 56, 1817-1822.	5.0	20
29	The motivations and methodology for high-throughput PET imaging of small animals in cancer research. European Journal of Nuclear Medicine and Molecular Imaging, 2012, 39, 1497-1509.	6.4	19
30	The impact of respiratory gated positron emission tomography on clinical staging and management of patients with lung cancer. Lung Cancer, 2015, 90, 217-223.	2.0	19
31	A 3D-printed anatomical pancreas and kidney phantom for optimizing SPECT/CT reconstruction settings in beta cell imaging using 111In-exendin. EJNMMI Physics, 2016, 3, 29.	2.7	19
32	Performance of automatic image segmentation algorithms for calculating total lesion glycolysis for early response monitoring in non-small cell lung cancer patients during concomitant chemoradiotherapy. Radiotherapy and Oncology, 2016, 119, 473-479.	0.6	17
33	Evaluation of different normalization procedures for the calculation of the standardized uptake value in therapy response monitoring studies. Nuclear Medicine Communications, 2009, 30, 550-557.	1.1	16
34	Characterization and optimization of image quality as a function of reconstruction algorithms and parameter settings in a Siemens Inveon small-animal PET scanner using the NEMA NU 4-2008 standards. Nuclear Instruments and Methods in Physics Research, Section A: Accelerators, Spectrometers, Detectors and Associated Equipment, 2011, 629, 357-367.	1.6	16
35	Tumor Delineation and Quantitative Assessment of Glucose Metabolic Rate within Histologic Subtypes of Non–Small Cell Lung Cancer by Using Dynamic ¹⁸ F Fluorodeoxyglucose PET. Radiology, 2017, 283, 547-559.	7.3	16
36	Scanning multiple mice in a small-animal PET scanner: Influence on image quality. Nuclear Instruments and Methods in Physics Research, Section A: Accelerators, Spectrometers, Detectors and Associated Equipment, 2010, 621, 605-610.	1.6	14

ERIC P VISSER

#	Article	IF	CITATIONS
37	Comparison of a Free-Breathing CT and an Expiratory Breath-Hold CT with Regard to Spatial Alignment of Amplitude-Based Respiratory-Gated PET and CT Images. Journal of Nuclear Medicine Technology, 2014, 42, 269-273.	0.8	13
38	Tumor and red bone marrow dosimetry: comparison of methods for prospective treatment planning in pretargeted radioimmunotherapy. EJNMMI Physics, 2015, 2, 5.	2.7	10
39	Performance of 3DOSEM and MAP algorithms for reconstructing low count SPECT acquisitions. Zeitschrift Fur Medizinische Physik, 2016, 26, 311-322.	1.5	10
40	Image quality phantom and parameters for high spatial resolution small-animal SPECT. Nuclear Instruments and Methods in Physics Research, Section A: Accelerators, Spectrometers, Detectors and Associated Equipment, 2011, 654, 539-545.	1.6	9
41	Whole organ and islet of Langerhans dosimetry for calculation of absorbed doses resulting from imaging with radiolabeled exendin. Scientific Reports, 2017, 7, 39800.	3.3	9
42	Evaluating the use of optimally respiratory gated 18F-FDG-PET in target volume delineation and its influence on radiation doses to the organs at risk in non-small-cell lung cancer patients. Nuclear Medicine Communications, 2016, 37, 66-73.	1.1	8
43	Comparison of liver SUV using unenhanced CT versus contrast-enhanced CT for attenuation correction in 18F-FDG PET/CT. Nuclear Medicine Communications, 2014, 35, 472-477.	1.1	7
44	Contribution of normalization to image noise for the Siemens Inveon small-animal PET scanner. Nuclear Instruments and Methods in Physics Research, Section A: Accelerators, Spectrometers, Detectors and Associated Equipment, 2009, 605, 433-435.	1.6	4
45	¹⁸ F-2-Deoxy-2-Fluoro-D-Glucose Positron Emission Tomography, Computed Tomography, and Magnetic Resonance Imaging for the Detection of Experimental Colorectal Liver Metastases. Molecular Imaging, 2012, 11, 7290.2011.00035.	1.4	2
46	Improving the Spatial Alignment in PET/CT Using Amplitude-Based Respiration-Gated PET and Patient-Specific Breathing–Instructed CT. Journal of Nuclear Medicine Technology, 2019, 47, 154-159.	0.8	2